Nonalcoholic fatty liver disease is associated with decreased hepatocyte mitochondrial respiration, but not mitochondrial number

Authors and affiliations: MC Sinton[1], J Meseguer Ripolles[2], B Lucendo Villarin[2], MJ Lyall[1], RN Carter[1], NM Morton[1], DC Hay[2], AJ Drake[1]

Corresponding author:

Amanda J. Drake: University/BHF Centre for Cardiovascular Science, Queen's Medical Research Institute, Edinburgh BioQuarter, 47 Little France Crescent, Edinburgh EH16 4TJ. mandy.drake@ed.ac.uk

Address:

1. University/BHF Centre for Cardiovascular Science, Queen's Medical Research Institute, Edinburgh BioQuarter, 47 Little France Crescent, Edinburgh EH16 4TJ
2. Scottish Centre for Regenerative Medicine, Edinburgh BioQuarter, 5 Little France Crescent, Edinburgh, EH16 4UU

Abstract

Nonalcoholic fatty liver disease (NAFLD) is currently the most prevalent form of liver disease worldwide. This term covers a spectrum of pathologies, from benign hepatic steatosis to non-alcoholic steatohepatitis (NASH). As the disease progresses, NASH can develop into cirrhosis and hepatocellular carcinoma. However, the underlying mechanisms and the factors which predispose an individual to disease progression remain poorly understood. Whilst NAFLD appears to be associated with mitochondrial dysfunction, it is unclear whether this is due to respiratory impairment, changes in mitochondrial mass, or mitochondrial fragmentation. Using a human pluripotent stem cell-based model of NAFLD we show that exposure to lactate, pyruvate and octanoic acid results in the development of macrovesicular steatosis. We do not observe changes in mitochondrial mass or fragmentation but do find decreases in maximal respiration and reserve capacity, suggesting impairment in the electron transport chain (ETC). Taken together, these findings indicate that the development of macrovesicular steatosis in NAFLD may be linked to the impairment of the ETC in mitochondria.

Introduction

Non-alcoholic fatty liver disease (NAFLD) is the most prevalent form of hepatic disease globally, estimated to affect 1 in 3 people. It is closely related to obesity, with ~88% of obese individuals at risk of developing the disease [1]. NAFLD is characterised by excess accumulation of triglycerides (TGs) in hepatocytes, leading to the development of steatosis [2]. Steatotic hepatocytes accumulate TGs in single large, or multiple medium-sized, cytoplasmic lipid droplets [3] and whilst simple steatosis is largely benign, its presence increases the risk of developing non-alcoholic steatohepatitis (NASH), which may progress to cirrhosis and hepatocellular carcinoma [4]. It is unclear why only a subset of patients develop NASH and, other than bariatric surgery for morbidly obese patients, there are currently no specific therapeutics available to treat or reverse this pathology [5].

Multiple studies suggest that the pathology of NAFLD is linked to impairment of mitochondrial function[6–9]. In rat models, mitochondrial dysfunction precedes the development of hepatic steatosis, suggesting that disease pathology and progression are linked to impairment of mitochondrial function [10]. NAFLD is linked to structural changes in mitochondrial cristae and the development of crystalline inclusion bodies [11]. As electron transport chain (ETC) components are embedded in the cristae, structural changes may have a physical impact on respiration [12]. Similarly, the growth of inclusion bodies may also impair oxidative phosphorylation and lead to increased free radical production [11]. This is supported by observations of NAFLD-associated hepatic oxidative stress and altered levels of fatty acid beta oxidation [11,12]. This is supported by the observation of NAFLD-associated hepatic oxidative stress and altered levels of fatty acid beta oxidation [11,12]. Furthermore, in humans, once hepatic lipid content exceeds 10%, lipid export is compromised [13]. In tandem with altered fatty acid beta oxidation, this imbalance may lead to the accumulation of intracellular lipids observed in NAFLD.

70 Satapati et al. (2012) observed increased tricarboxylic acid (TCA) cycle activity and
71 anaplerosis in the livers of mice with high fat diet-induced hepatic steatosis [7]. They also
72 demonstrate that increased levels of hepatic TGs induced oxidative metabolism, with a
73 proportional increase in oxidative stress [14]. Indirect studies in humans indicate a similar
74 effect on TCA cycle flux [6]. As TCA cycle flux generates NADH and $FADH_2$, which transfer
75 electrons to the electron transport chain (ETC), alterations in TCA cycling may have a direct
76 impact on respiration and oxidative stress. Further studies in humans demonstrate that
77 NAFLD and NASH are associated with increased and decreased mitochondrial maximal
78 respiration, respectively, indicating that there is a transition in mitochondrial function
79 between these two disease states [15]. The reasons for this are unclear; such differences in
80 maximal respiration between NAFLD and NASH could reflect impairment of the ETC and/or
81 changes in baseline mitochondrial respiration. Furthermore, mitochondria isolated from
82 whole tissue come from multiple cell types, which may differ in proportion in disease states
83 and this may confound the interpretation of any results. Observations that mitochondrial
84 mass increased in NASH with a concomitant decrease in maximal respiration may also arise
85 from organelle fragmentation, a phenotype associated with oxidative stress and apoptosis in
86 other diseases [16].
87
88 In light of current knowledge, we hypothesised that nutrient excess in NAFLD leads to
89 mitochondrial dysfunction and subsequent increases in ETC activity due to increased
90 availability of respiratory substrates. Therefore, we aimed to determine the impact of lipid
91 accumulation on mitochondrial respiration specifically in hepatocytes, to avoid the
92 confounding effects associated with bulk tissue analysis. We also aimed to determine
93 whether changes in respiration were related to altered mitochondrial mass or fragmentation.
94 To this end, we used a recently developed *in vitro* model of NAFLD [17] to explore the
95 impact of hepatic steatosis on mitochondrial respiration.

Methods

Differentiation of pluripotent human stem cells to hepatocyte-like cells and induction of intracellular lipid accumulation

Human female H9 pluripotent stem cells (PSCs) were differentiated to hepatocyte-like cells (HLCs) as previously described [18]. HLCs were cultured in a 96-well format for measurements of lipid accumulation and in a 6-well format for all other analyses. Intracellular lipid accumulation was induced in HLCs, as previously described [17]. Briefly, at day 17, HLCs were exposed to a cocktail of sodium l-lactate (L; 10mM), sodium pyruvate (P; 1 mM) and octanoic acid (O; 2 mM) (Sigma, Gillingham, UK).

High content analysis microscopy

Cells were stained with a cell painter assay, adapted from Lyall *et al* and Bray *et al* [17,19]. Cells were fixed with 50 µL/well 4% (wt/vol) paraformaldehyde (Electron Microscopy Sciences, 15710-S) for 15 minutes at room temperature. For permeabilisation, cells were incubated in 0.1% Triton X-100 (Sigma-Aldrich, T8787) in PBS for 15 minutes at room temperature. For lipid droplet analysis, cells were then stained with a combination of NucBlue Live ReadyProbes® Reagent (2 drops/mL) (Molecular Probes, R37605), HCS CellMask™ Red (2 µL/10 mL) (Invitrogen, H32712), and BODIPY™ 493/503 (1:1000) (Life Sciences, D3922), as per the manufacturer's instructions. For mitochondrial quantification, cells were stained with a combination of NucBlue Live ReadyProbes® Reagent (2 drops/mL), MitoTracker™ Deep Red FM (1/4000; Invitrogen, M22426), and Alexa Fluor™ 555 Phalloidin (Invitrogen, A34055). Following staining, images were acquired using an Operetta High Content Analysis microscope (Perkin Elmer, Buckinghamshire, UK). Lipid droplet morphology was analysed as previously described [17].

122

123 **Cell mitochondrial stress test assay**

124 The oxygen consumption rate (OCR) of LPO-exposed HLCs was measured using the
125 Agilent Seahorse XF Cell Mito Stress Test Kit (Agilent, 103015-100) on a Seahorse XF
126 Analyser (Agilent, California, USA). Analysis was performed under basal conditions, and
127 following treatment with oligomycin A (an ATPase inhibitor), carbonyl-cyanide-4-
128 (trifluoromethoxy) phenylhydrazone (FCCP; an ETC uncoupler), and combined rotenone and
129 antimycin A (inhibitors of complex I and III, respectively). Two concentrations of FCCP (0.5
130 µM and 1.0 µM) were used for optimisation. Since replicates within each group responded
131 similarly to each other, results were combined. OCR was normalised to total protein for each
132 well, using the sulforhodamine B (SRB) assay, as previously described [20], but with
133 spectrophotometric measurements read at 540 nm.

134

135 **Citrate synthase assay**

136 Mitochondria were isolated using the Mitochondria Isolation Kit for Cultured Cells (Thermo
137 Scientific, 89874), as per the manufacturer's instructions, selecting option A for isolation.
138 Citrate synthase activity, a marker for mitochondrial integrity, was then measured using the
139 Citrate Synthase Activity Colorimetric Assay Kit (BioVision, K318), as per the manufacturer's
140 instructions.

141

142 **Protein Extraction**

143 Adherent HLCs were washed once with ice-cold PBS, before incubating in ice-cold RIPA
144 Lysis and Extraction Buffer (Thermo Scientific, 89900) supplemented with cOmplete™
145 Protease Inhibitor Cocktail tablets (1/10 mL buffer; Roche, 11697498001). The suspended
146 HLCs were placed on ice for 30 minutes, vortexing every 3 minutes, before centrifuging for

147 20 min at 4 °C, 12,000 rpm. The supernatant was collected and stored at -80 °C until
148 needed.
149
150 **Western blot analysis**
151 Protein quantification was performed using the Qubit™ Protein Assay Kit (Invitrogen,
152 Q33211), as per the manufacturer's instructions. Protein concentration was measured using
153 a Qubit™ Fluorometer (Invitrogen, Massachusetts, USA). Equal concentrations (50 µg) of
154 HLC protein extract in 4 x Sample Loading Buffer (Li-Cor, 928-40004) were loaded onto
155 NuPAGE™ 4-12% Bis-Tris Protein Gels (Invitrogen, NP0326BOX). Following resolution,
156 protein was transferred to a methanol-activated polyvinylidene difluoride (PVDF) membrane.
157 Protein transfer was measured using Revert 700 Total Protein Stain Kit (Li-Cor, 926-11010)
158 as per the manufacturer's instructions. Membranes were then blocked with Tris-buffered
159 saline containing Tween 20 (TBST) and 5% skimmed milk powder, before incubating with
160 either Pyruvate Dehydrogenase (C54G1) Rabbit mAb (Cell Signaling Technology, 3205) or
161 SDHA (D6J9M) XP® Rabbit mAb (Cell Signaling Technology, 11998), both a 1:1000 dilution.
162 The membranes were washed in TBST before incubating with the secondary antibody,
163 IRDye® 680RD Donkey anti-Mouse IgG (Li-Cor, 926-68072) at a 1:10,000 dilution, for 1 h at
164 room temperature, in the dark, with shaking. Blots were visualised on a Li-Cor Odyssey®
165 CLx (Li-Cor, Nebraska, USA), and bands normalised to the Revert 700 Total Protein Stain,
166 as per the manufacturer's instructions.
167
168 **Real-time quantitative PCR**
169 Total RNA was extracted from HLCs using the Monarch® Total RNA Miniprep Kit (New
170 England BioLabs, T2010). cDNA was generated using the High Capacity cDNA Reverse
171 Transcriptase Kit (Applied Biosystems, 4368814). A master mix was prepared using
172 PerfeCTa FastMix II (Quanta Biosciences, Inc., 95118-250). cDNA was amplified and

173 quantified using the Universal Probe Library (Roche, Burgess Hill, UK) system on a Roche
174 LightCycler 480 (Roche Diagnostics Ltd, Switzerland). Details of primers and Universal
175 Probe Library probes (Roche) and primers used can be found in Table S1.

176 **Measurement of mitochondrial and nuclear DNA**

177 DNA was extracted from HLCs using the Monarch® Genomic DNA Purification Kit (New
178 England BioLabs, T3010). A master mix was prepared using the Luna® Universal qPCR
179 Master Mix (New England BioLabs, M3003). DNA was amplified and quantified using a
180 Roche LightCycler 480 (Roche Diagnostics Ltd, Switzerland). Primers were designed
181 against two regions of the NCBI mitochondrial reference sequence NC_012920.1, and one
182 region of the genomic reference sequence NC_000011.10. Primers used can be found in
183 Table S2.

184

185 **Statistical analyses**

186 All statistical analyses were performed using Graph Prism Version 8.0 for Windows or
187 macOS, GraphPad Software, La Jolla California USA, www.graphpad.com. Normality of
188 data distribution was measured using the Shapiro-Wilks test. Normally distributed data were
189 analysed using a parametric unpaired Student's t-test, and non-normally distributed data
190 were analysed using a non-parametric Mann-Whitney test. Data were considered to be
191 significant where $p < 0.05$.

192

193 **Results**

194 **LPO-treatment induces macrovesicular steatosis in HLCs**

195 We previously reported that the high energy substrate cocktail LPO promotes intracellular
196 lipid accumulation in HLCs [17] although it was not known whether LPO promotes lipid
197 droplet biogenesis or increased accumulation of lipids within existing droplets. Stem cell
198 derived HLCs were differentiated and characterised as before [18] (Figure 1A). Analysis of
199 gene expression using RT-qPCR showed increased expression of transcripts for PLIN2,
200 PLIN4, and PLIN5, which are typically associated with intracellular lipid droplet membranes,
201 suggesting an increase in lipid droplet size (Figure 1B-D). Analysis of lipid accumulation
202 using high content imaging (Figure 1E) demonstrated that LPO exposure was not associated
203 with a change in the number of lipid droplets (Figure 1F), but led to a ~2-fold increase in the
204 size of intracellular lipid droplets (Figure 1G), consistent with the development of
205 macrovesicular steatosis.

206

207 **Macrovesicular steatosis in hepatocytes is associated with electron transport chain**
208 **dysfunction**

209 It has been suggested that NAFLD-associated macrovesicular steatosis results in
210 impairment of mitochondrial respiration and we therefore proceeded to analyse this in
211 steatotic HLCs (Figure 2A). Basal oxygen consumption rate (OCR), representing combined
212 mitochondrial and non-mitochondrial oxygen consumption, was unchanged following LPO
213 exposure (Figure 2B). Additionally, oligomycin A, a complex V inhibitor decreased OCR
214 equally effectively in control and treatment group. Firstly, this indicated that there were no
215 changes in ATP-linked respiration in response to macrovesicular steatosis (Figure 2C).
216 Secondly, when comparing oligomycin A-induced alterations in OCR with those following
217 addition of rotenone/antimycin A, we could detect no changes in proton leak between groups
218 (Figure 2D). The addition of the ETC uncoupler FCCP revealed a decrease in maximal

219 respiration in the steatotic HLCs, suggesting ETC dysfunction (Figure 2E). Using OCR
220 measurements following FCCP treatment, and comparing to the basal OCR, we calculated
221 that there was a decrease in reserve capacity in the LPO-treated cells, compared with
222 controls (Figure 2F). Subsequently, complex I and III were targeted with rotenone/antimycin
223 A, to completely inhibit oxidative phosphorylation, which reduced OCR to a similar level in
224 both groups, suggesting no difference in non-mitochondrial sources of OCR between the
225 control and steatotic HLCs.
226
227 **Induction of macrovesicular steatosis is not associated with mitochondrial**
228 **fragmentation or alterations in mitochondrial number**
229 To analyse whether the observed changes in OCR could be due to mitochondrial
230 fragmentation rather than ETC dysfunction we measured citrate synthase (CS) activity. LPO
231 treatment had no impact on CS activity (Figure 3A), suggesting that mitochondria remain
232 intact following intracellular lipid accumulation. A final question was whether changes in ETC
233 function, as demonstrated by decreased cellular maximal respiration and reserve capacity,
234 were due to decreased numbers of mitochondria in response to intracellular lipid
235 accumulation. Since these were the only respiratory measurements to change, we
236 hypothesised that this was not the case. We first measured protein levels of succinate
237 dehydrogenase subunit A (SDHA) and pyruvate dehydrogenase (PDH) (Figure 3B), which
238 localise to the mitochondria. Protein levels of SDHA and PDH did not change in response to
239 intracellular lipid accumulation, suggesting that mitochondrial number is not altered by LPO-
240 induced macrovesicular steatosis. Furthermore, there were no changes in mitochondrial or
241 nuclear DNA (Figure 3C) and no change in the ratio of nuclear to mitochondrial DNA (Figure
242 3D). Finally, we used a high content microscopy-based approach to measure intracellular
243 mitochondrial quantity (Figure 3E), and observed no changes following exposure to LPO

244 (Figure 3F). Taken together, these data suggest that mitochondrial number is not altered in

245 the presence of intracellular lipid accumulation.

246

247 **Discussion**

248 In this study we aimed to determine the nature of NAFLD-associated changes in
249 mitochondrial respiration, and whether these occur as a result of mitochondrial dysfunction
250 or reductions in mitochondrial number. Using a combination of high content microscopy and
251 gene expression analyses, we first confirmed that treatment of HLCs with LPO induced
252 intracellular lipid accumulation (Figure 1). The observed changes in the expression of genes
253 associated with lipid droplet size (PLIN2, 4 and 5) are also in agreement with findings from
254 human studies with intracellular lipid accumulation associated with an upregulation of PLIN2
255 in human hepatocytes [21] and biopsies from NAFLD patients [22]. In adipocytes, PLIN4
256 localises to the surface of unilocular lipid droplets, and may participate in their early
257 development. Although there are no human studies describing perturbed expression of
258 PLIN4 in association with NAFLD, its knockout protects against liver steatosis in mice [23].
259 Furthermore, PLIN4 knockout diminishes the accumulation of triacylglycerol in lipid droplets
260 and reduces the expression of PLIN5 in mouse cardiac tissue. Therefore, their interplay may
261 be important for the pathology of NAFLD. In support of this, *in vitro* studies show that PLIN5
262 blocks lipid droplet lipolysis in hepatocytes and an increase in PLIN5 expression may
263 therefore contribute to the development of macrovesicular steatosis [24]. Increases in the
264 expression of PLIN2, PLIN4 and PLIN5 in LPO-treated HLCs, alongside BODIPY staining,
265 strongly indicate that this model recapitulates macrovesicular steatosis observed in humans
266 with NAFLD.

267

268 Following the further establishment of relevance to human disease, we wished to
269 understand whether macrovesicular steatosis was linked to dysfunction of mitochondrial
270 respiration [15]. Previous studies have shown that mitochondrial maximal respiration
271 increases in obese humans with NAFLD but decreases on progression to NASH, despite an
272 increase in mitochondrial mass. In contrast to the initial hypothesis, we observed decreased

273 maximal respiration and reserve capacity in cells displaying a NAFLD phenotype. This
274 indicates that whilst mitochondria are mostly able to maintain respiratory integrity in LPO-
275 exposed cells, the ETC, and therefore oxidative phosphorylation, may be compromised.
276 Given that these were the only parameters of mitochondrial respiration to change, it
277 suggests that LPO treatment of HLCs inhibits complexes I-III of the ETC. This effect may
278 arise due to the use of octanoic acid, which inhibits complex I-III in rat liver, as well as
279 increasing oxidative stress through reactive oxygen species production [25]. Inhibition of
280 complex II may also impact on the TCA cycle, potentially altering its function, and the
281 generation of cofactors necessary for oxidative phosphorylation, further impacting on cellular
282 metabolism. However, further studies are required to test these hypotheses.
283
284 Finally, we questioned whether changes in maximal respiration arose from fragmentation of
285 mitochondria or resulted from increased biogenesis. Given that maximal respiration was the
286 only parameter of respiration that changed, we suspected this was not the case. This was
287 confirmed by lack of change in the ratio of nuclear to mitochondrial DNA, suggesting that
288 mitochondrial biogenesis was not affected by LPO treatment in these studies. This is
289 consistent with human studies of NAFLD which show no changes in mitochondrial mass in
290 steatotic versus non-steatotic liver tissue [15]. In contrast, liver tissue from patients with
291 NASH contains greater numbers of mitochondria, with a concomitant decrease in maximal
292 respiration. Therefore, the model of NAFLD presented here may mirror the transition
293 between NAFLD and NASH, with respiratory dysfunction in the absence of mitochondrial
294 biogenesis. This discrepancy may also be due to previous studies using isolated
295 mitochondria from whole tissues, comprised of multiple cell types, whereas we examined a
296 single cell population.
297

298 In conclusion, here we demonstrate that the treatment of HLCs with LPO induces
299 intracellular lipid accumulation in patterns similar to those observed in human pathology.
300 Furthermore, we observed decreased mitochondrial maximal respiration, in the absence of
301 altered mitochondrial biogenesis. Taken together, our data demonstrate that hepatocyte
302 intracellular lipid accumulation is linked to mitochondrial dysfunction in response to the
303 changing bioenergetic demands associated with NAFLD, impacting on the ETC, and limiting
304 maximal respiration.
305

306 **Acknowledgements**

307 MCS was supported by a British Heart Foundation PhD studentship (FS/16/54/32730) and
308 by the BHF Centre of Research Excellence. BLV and DCH were supported by an award
309 from the Chief Scientist Office (TCS/16/37). JMR was supported by an MRC PhD
310 studentship. MJL was supported by a Wellcome Trust PhD studentship as part of the
311 Edinburgh Clinical Academic Track (102839/Z/13/Z). RNC and NMM were supported by a
312 Wellcome Trust New Investigator Award to NMM (100981/Z/13/Z). AJD was supported by
313 the BHF Centre of Research Excellence, Edinburgh. We thank Will Cawthorn for discussions
314 about mitochondrial quantification.

315

316 **Author contributions**

317 MCS, JMR, BLV, MJL, RNC and NMM performed experiments. DCH and AJD conceived the
318 experiments. MCS, NMM, DCH and AJD wrote the paper. All authors contributed to drafts of
319 the paper and approved the final version.

320

321 **Declaration of Interests**

322 Professor David C Hay is a co-founder, shareholder and director of Stemnovate Limited

323

324 **Figure Legends**

325 Figure 1. LPO treatment induces development of macrovesicular lipid droplets. (**A**) H9
326 hPSCs differentiate to HLCs, losing pluripotency and gaining expression of the hepatic
327 markers albumin and HNF4A (n = 3 biological replicates/group); (**B-D**) PLIN2, PLIN4, and
328 PLIN5 expression increases in response to LPO treatment (n = 3 biological replicates per
329 group). (**E**) Representative images of lipid accumulation in control & LPO-treated groups 10x
330 magnification. (**F**) Number of lipid droplets do not increase, (**G**) but intracellular lipid droplets
331 increase in size (n = 32 biological replicates/group). Data analysed using two-tailed Student
332 t-test and expressed as mean ± SD, *p<0.05, ****p<0.0001.

333

334 Figure 2. LPO treatment results in decreased maximal respiration in mitochondria but not in
335 other aspects of oxygen consumption rate. HLCs were injected sequentially from ports A-C
336 with 4 μM oligomycin, 0.5-1 μM FCCP, and 1 μM antimycin combined with 200 nM rotenone.
337 (**A**) Raw trace of OCR comparing cells with or without LPO treatment; (**B**) basal respiration;
338 (**C**) ATP-linked respiration; (**D**) proton leak; (**E**) maximal respiration; (**F**) reserve capacity
339 compared to control treatment (n = 18 and 16 biological replicates in the control and
340 treatment group, respectively). Data analysed using two-tailed Student t-test for parametric
341 data, or Mann-Whitney U test for non-parametric data, and expressed as mean ± SD.

342

343 Figure 3. LPO does treatment does induce mitochondrial fragmentation or change
344 mitochondrial number. (**A**) Levels of citrate synthase activity were unaltered by LPO
345 treatment (n = 3 biological replicates/group); (**B**) Protein levels of succinate dehydrogenase
346 subunit A (SDHA) and pyruvate dehydrogenase were unchanged (n = 6 biological
347 replicates/group); (**C**) no changes were observed in abundance of DNA in mitochondrial
348 region 2 (MT2); mitochondrial region 3 (MT3); or genomic region beta-globin (HBB); (**D**)
349 there were no significant changes in the ratio of mitochondrial to genomic DNA, indicating no

350 alterations in the quantity of mitochondria in response to treatment (n=4 biological
351 replicates/group for **C** and **D**); (**E**) Representative images of mitochondrial content in control
352 & LPO-treated groups 10x magnification. Blue staining = NucBlue, red staining =
353 MitoTracker Deep Red; (**F**) high content microscopy revealed no changes in mitochondrial
354 quantity in response to treatment (n = 4 and 6 biological replicates in the control and
355 treatment group, respectively). Data analysed using two-tailed Student t-test for parametric
356 data, or Mann-Whitney U test for non-parametric data, and expressed as mean ± SD.
357
358 **Supplementary materials S1**.
359 Primer sequences and UPL probes used for qPCR assays

360 **References**

361 1. World Health Organization. Obesity and overweight. https://www.who.int/news-
362 room/fact-sheets/detail/obesity-and-overweight (2018).
363 2. Valenti, L., Bugianesi, E., Pajvani, U. & Targher, G. Nonalcoholic fatty liver disease:
364 cause or consequence of type 2 diabetes? *Liver International* vol. 36 1563–1579
365 (2016).
366 3. Wang, L. & Yu, S. Pathology of non-alcoholic fatty liver disease. *Int. J. Dig. Dis.* **2**,
367 (2016).
368 4. Asrih, M. & Jornayvaz, F. R. Metabolic syndrome and nonalcoholic fatty liver disease:
369 Is insulin resistance the link? *Molecular and Cellular Endocrinology* vol. 418 55–65
370 (2015).
371 5. Laursen, T. L. *et al.* Bariatric surgery in patients with non-alcoholic fatty liver disease -
372 From pathophysiology to clinical effects. *World Journal of Hepatology* vol. 11 138–249
373 (2019).
374 6. Sunny, N. E., Parks, E. J., Browning, J. D. & Burgess, S. C. Excessive hepatic
375 mitochondrial TCA cycle and gluconeogenesis in humans with nonalcoholic fatty liver
376 disease. *Cell Metab.* **14**, 804–810 (2011).
377 7. Satapati, S. *et al.* Elevated TCA cycle function in the pathology of diet-induced hepatic
378 insulin resistance and fatty liver. *J. Lipid Res.* **53**, 1080–1092 (2012).
379 8. Patterson, R. E. *et al.* Lipotoxicity in steatohepatitis occurs despite an increase in
380 tricarboxylic acid cycle activity. *Am. J. Physiol. - Endocrinol. Metab.* **310**,
381 ajpendo.00492.2015 (2016).
382 9. Sunny, N. E., Bril, F. & Cusi, K. Mitochondrial adaptation in nonalcoholic fatty liver
383 disease: novel mechanisms and treatment strategies. *Trends Endocrinol. Metab.* **28**,
384 250–260 (2017).
385 10. Rector, R. S. *et al.* Mitochondrial dysfunction precedes insulin resistance and hepatic

386 steatosis and contributes to the natural history of non-alcoholic fatty liver disease in
387 an obese rodent model. *J. Hepatol.* **52**, 727–736 (2010).
388 11. Sanyal, A. J. *et al.* Nonalcoholic steatohepatitis: association of insulin resistance and
389 mitochondrial abnormalities. *Gastroenterology* **120**, 1183–1192 (2001).
390 12. Caldwell, S. H. *et al.* Mitochondrial abnormalities in non-alcoholic steatohepatitis. *J.*
391 *Hepatol.* **31**, 430–434 (1999).
392 13. Fabbrini, E. *et al.* Alterations in adipose tissue and hepatic lipid kinetics in obese men
393 and women with nonalcoholic fatty liver disease. *Gastroenterology* **134**, 424–431
394 (2008).
395 14. Satapati, S. *et al.* Mitochondrial metabolism mediates oxidative stress and
396 inflammation in fatty liver. *J. Clin. Invest.* **125**, 4447–4462 (2015).
397 15. Koliaki, C. *et al.* Adaptation of hepatic mitochondrial function in humans with non-
398 alcoholic fatty liver is lost in steatohepatitis. *Cell Metab.* **21**, 739–746 (2015).
399 16. Knott, A. B., Perkins, G., Schwarzenbacher, R. & Bossy-Wetzel, E. Mitochondrial
400 fragmentation in neurodegeneration. *Nature Reviews Neuroscience* vol. 9 505–518
401 (2008).
402 17. Lyall, M. J. *et al.* Modelling non-alcoholic fatty liver disease in human hepatocyte-like
403 cells. *Philos. Trans. R. Soc. B Biol. Sci.* **373**, 20170362 (2018).
404 18. Wang, Y. *et al.* Defined and scalable generation of hepatocyte-like cells from human
405 pluripotent stem cells. *J. Vis. Exp.* e55355–e55355 (2017).
406 19. Bray, M. A. *et al.* Cell Painting, a high-content image-based assay for morphological
407 profiling using multiplexed fluorescent dyes. *Nat. Protoc.* **11**, 1757–1774 (2016).
408 20. Orellana, E. & Kasinski, A. Sulforhodamine B (SRB) assay in cell culture to
409 investigate cell proliferation. *Bio-Protocol* **6**, (2016).
410 21. Sahini, N. & Borlak, J. Genomics of human fatty liver disease reveal mechanistically
411 linked lipid droplet–associated gene regulations in bland steatosis and nonalcoholic

412 steatohepatitis. *Transl. Res.* **177**, 41–69 (2016).

413 22. Fujii, H. *et al.* Expression of perilipin and adipophilin in nonalcoholic fatty liver disease;
414 relevance to oxidative injury and hepatocyte ballooning. *J. Atheroscler. Thromb.* **16**,
415 893–901 (2009).

416 23. Chen, W. *et al.* Inactivation of Plin4 downregulates Plin5 and reduces cardiac lipid
417 accumulation in mice. *Am. J. Physiol. - Endocrinol. Metab.* **304**, E770-9 (2013).

418 24. Wang, C. *et al.* Perilipin 5 improves hepatic lipotoxicity by inhibiting lipolysis.
419 *Hepatology* **61**, 870–882 (2015).

420 25. Scaini, G. *et al.* Toxicity of octanoate and decanoate in rat peripheral tissues:
421 evidence of bioenergetic dysfunction and oxidative damage induction in liver and
422 skeletal muscle. *Mol. Cell. Biochem.* **361**, 329–335 (2012).

423
424
425
426
427
428
429
430
431
432
433
434
435
436
437

Figure 1

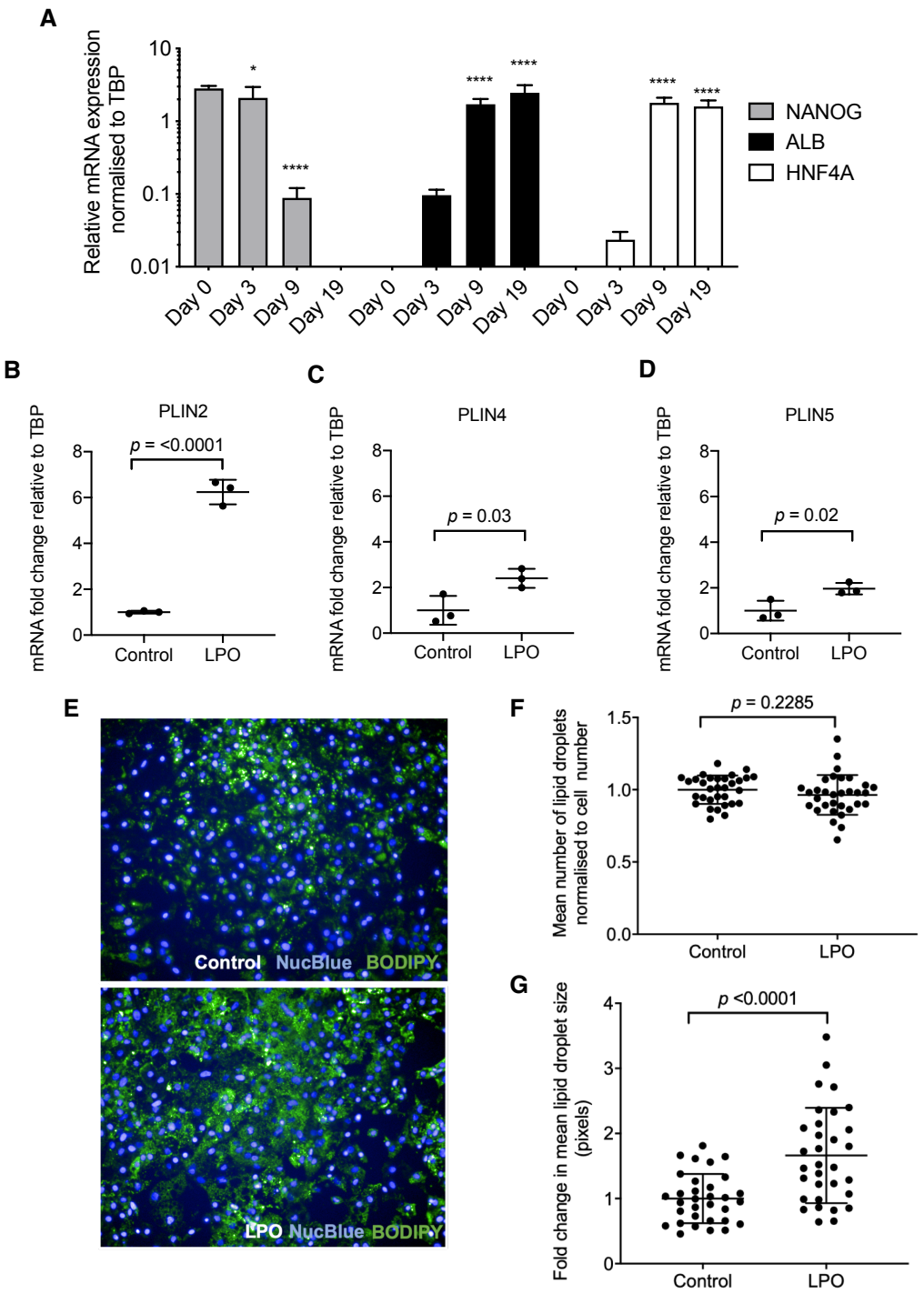
A
Relative mRNA expression normalised to TBP
10
1
0.1
0.01
*
****
****
****
****
****
NANOG
ALB
HNF4A
Day 0
Day 3
Day 9
Day 19
Day 0
Day 3
Day 9
Day 19
Day 0
Day 3
Day 9
Day 19
B
PLIN2
p = <0.0001
mRNA fold change relative to TBP
Control
LPO
C
PLIN4
p = 0.03
mRNA fold change relative to TBP
Control
LPO
D
PLIN5
p = 0.02
mRNA fold change relative to TBP
Control
LPO
E
Control NucBlue BODIPY
LPO NucBlue BODIPY
F
p = 0.2285
Mean number of lipid droplets normalised to cell number
Control
LPO
G
p <0.0001
Fold change in mean lipid droplet size (pixels)
Control
LPO

438

Figure 2

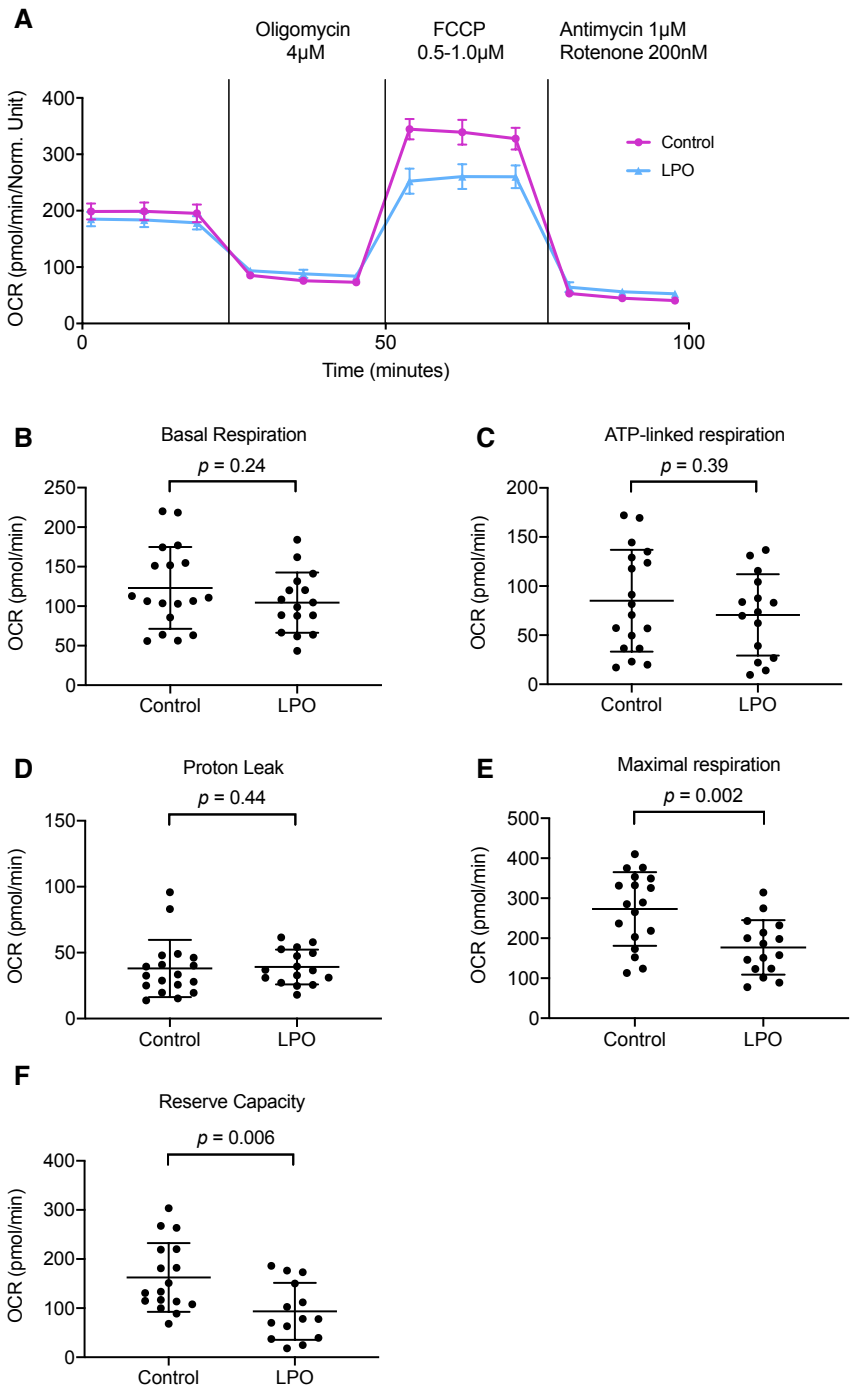
A
Oligomycin
4μM
FCCP
0.5-1.0μM
Antimycin 1μM
Rotenone 200nM
OCR (pmol/min/Norm. Unit)
Time (minutes)
Control
LPO
B
Basal Respiration
p = 0.24
OCR (pmol/min)
Control
LPO
C
ATP-linked respiration
p = 0.39
OCR (pmol/min)
Control
LPO
D
Proton Leak
p = 0.44
OCR (pmol/min)
Control
LPO
E
Maximal respiration
p = 0.002
OCR (pmol/min)
Control
LPO
F
Reserve Capacity
p = 0.006
OCR (pmol/min)
Control
LPO

439

Figure 3

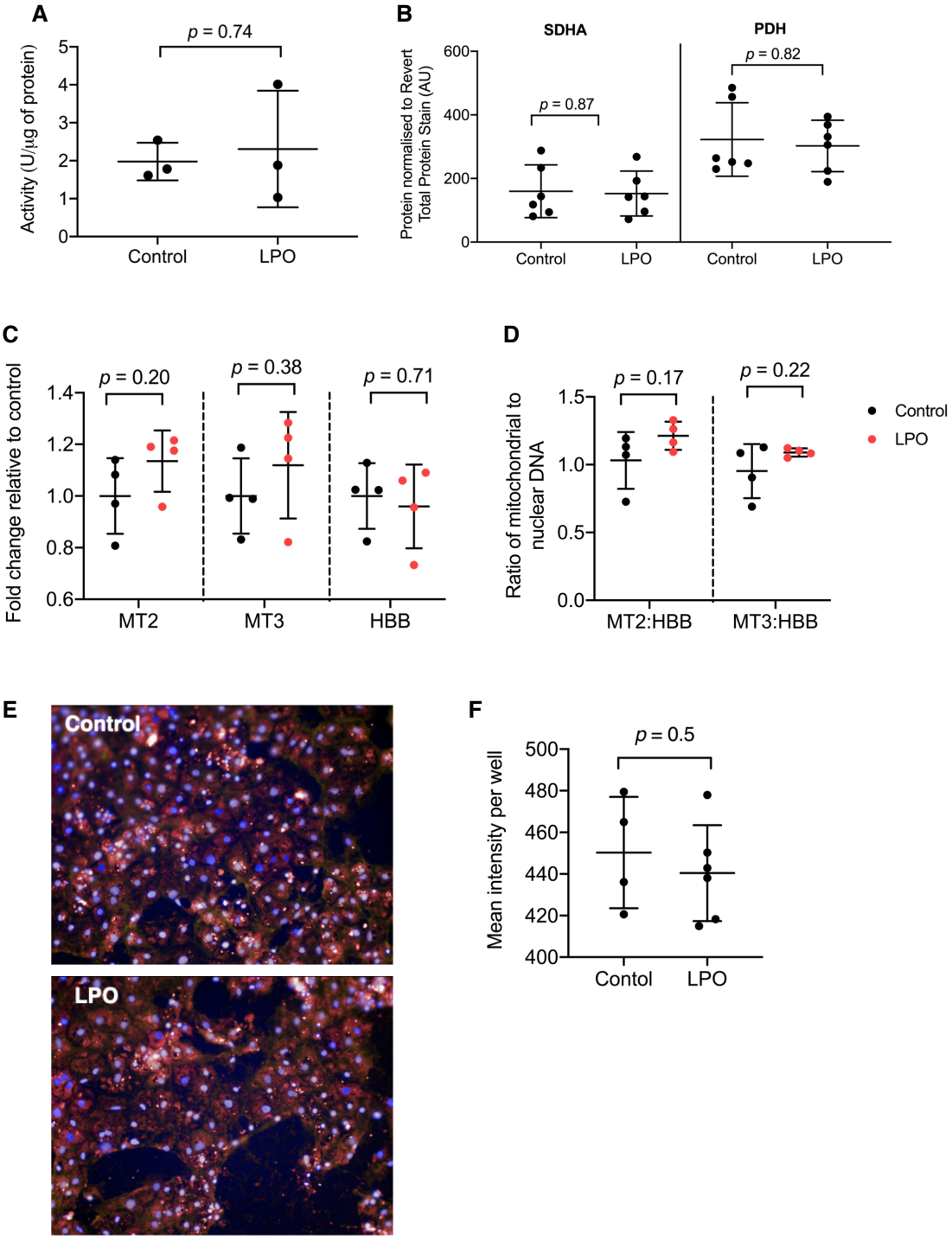
A
p = 0.74
Activity (U/µg of protein)
5
4
3
2
1
0
Control
LPO
B
SDHA
PDH
p = 0.87
p = 0.82
Protein normalised to Revert Total Protein Stain (AU)
600
400
200
0
Control
LPO
Control
LPO
C
Fold change relative to control
p = 0.20
p = 0.38
p = 0.71
1.4
1.2
1.0
0.8
0.6
MT2
MT3
HBB
D
Ratio of mitochondrial to nuclear DNA
p = 0.17
p = 0.22
1.5
1.0
0.5
0.0
MT2:HBB
MT3:HBB
Control
LPO
E
Control
LPO
F
Mean intensity per well
p = 0.5
500
480
460
440
420
400
Contol
LPO

440